Energy Reports 7 (2021) 654–666

Contents lists available at ScienceDirect

Energy Reports

journal homepage: www.elsevier.com/locate/egyr

Impact of integrating large-scale DFIG-based wind energy conversion system on the voltage stability of weak national grids: A case study of the Nigerian power grid

Bukola Babatunde Adetokun [a,*], Christopher Maina Muriithi [b]

[a] Department of Electrical Engineering, PAU Institute for Basic Sciences, Technology and Innovation, Jomo Kenyata University of Agriculture and Technology, Juja, Nairobi, Kenya
[b] Department of Electrical Engineering, Murang'a University of Technology, Murang'a, Kenya

ARTICLE INFO

Article history:
Received 17 September 2020
Received in revised form 2 January 2021
Accepted 14 January 2021
Available online xxxx

Keywords:
Active power margin
DFIG
Reactive power margin
Voltage stability
Wind energy conversion system

ABSTRACT

This paper investigates the impact of integrating large-scale Doubly-Fed Induction Generator (DFIG)-based wind energy conversion system (WECS) on the voltage stability of the 52-bus, 330 kV Nigerian power grid. Indices derived from Active Power–Voltage (PV) and Reactive Power–Voltage (QV) analyses have been utilized to determine the voltage stability limits in terms of the maximum active power margin (APM) and minimum reactive power margin (RPM) of the system with the associated critical voltage-reactive power ratio (CVQR) of the system buses. Simulations have been done in DIgSILENT PowerFactory and the results analysed using MATLAB. This work also demonstrates the effectiveness of DFIG-based WECS in mitigating the overvoltage issues in the Northern region by ensuring that all bus voltages are within the acceptable limits of 1.0 ± 0.05 p.u. The results show that the optimal DFIG-based WECS penetration level (PL) that satisfies a bus voltage criterion of 1.0 ± 0.05p.u with the APM and CVQR not falling below their respective base case values and the loading of all critical power system equipment not exceeding 80% is 35%. Therefore, this work has demonstrated the possibilities of large-scale DFIG-based WECS as a viable solution for voltage stability improvement of a weak National grid while meeting the increasing energy demand.

1. Introduction

The subject of harnessing renewable energy (RE) resources for a sustainable power and energy sector has become popular in recent decades. This drive towards sustainable and renewable power generation has been accelerated by the obvious necessity to serve the rising global energy demand while significantly reducing dependence on fossil-fuels (Ayodele et al., 2017; Jacobson et al., 2018; Ogunjuyigbe et al., 2017; Ahmad et al., 2020). Thus, design and development of renewable and sustainable energy systems has witnessed remarkable progress in different parts of the world, where large-scale RE integration into the existing grid is becoming more viable. Wind Energy Conversion Systems (WECS) is the most widely utilized renewable alternatives at present, with over 591 GW of wind energy conversion systems installed globally (Adetokun et al., 2020a).

Several studies have been carried out on the impact of wind turbine generators on grid voltage stability (Adetokun et al., 2020a; Raghavendran et al., 2020; Kaloi et al., 2016; Chen et al., 2017; Bennouk et al., 2018; Willenberg et al., 2020; Rahimi, 2017; Adetokun et al., 2020b; Heetun et al., 2016; Jadidbonab et al., 2019; da Costa et al., 2019; Bian et al., 2016). In Chen et al. (2017), the mechanism for stability and fast control of power system integrated with wind energy has been examined. It was shown that voltage stability challenge is more obvious than rotor-angle stability when there is increased penetration of wind energy and an emergency control scheme was developed to address the transient voltage instability due to increased wind energy penetration. The authors in Rahimi (2017) studied the use of coordinated rotor and grid-side converters in a DFIG-based wind turbine in order to provide voltage support for the grid. This approach was also applied for voltage profile improvement and mitigation of voltage fluctuations. The studies in Adetokun et al. (2020a) and (Adetokun et al., 2020b) dealt with the assessment and improvement of voltage stability of wind integrated power systems considering doubly-fed induction generator and squirrel-cage induction generator respectively. In addition, the impact of large wind integration on loading margin sensitivities of a wind-connected power system has been studied in da Costa et al. (2019).

* Corresponding author.
E-mail addresses: jesutunde@gmail.com, adetokun.bukola@students.jkuat.ac.ke (B.B. Adetokun).

https://doi.org/10.1016/j.egyr.2021.01.025

Some analysis regarding the impact of wind energy and other renewable integration on the national grid of developed countries have been carried out in Esteban et al. (2018), Wu et al. (2016), Xia et al. (2015), Modi et al. (2013), Astiaso Garcia and Bruschi (2016), Noorollahi et al. (2017), Yan et al. (2015), Waewsak et al. (2017), Ciupăgeanu et al. (2019), Feilat et al. (2018), Carvajal-Romo et al. (2019), Johnson et al. (2020), Wang et al. (2020), Wiser et al. (2016), Zhang et al. (2019), Bayer and Marian (2020). The authors in Xia et al. (2015) investigated the possible stability challenges that may arise in the future United Kingdom power grid with high wind energy penetration level. In Esteban et al. (2018), an assessment on the feasibility of a 100% renewable energy grid in Japan was carried out by considering scenarios of future wind, solar and tidal energy production. The results show that system stability can be possible with the required incorporation of energy storage. The effects of large-scale wind energy generation on the stability of Australia's Queensland was investigated in Modi et al. (2013), considering the state's expectation of high wind energy penetration in its Northern region. Also, the aggregate effects of high share of wind and solar PV on the frequency response of South Australia's power system was studied in Yan et al. (2015). In Ciupăgeanu et al. (2019), the variability analysis and impact of wind energy integration on the Romanian grid has been analysed using historic records of more than 10 years. Also, the impact of utility-scale PV and WECS on the voltage and frequency stability of Jordan national grid has been investigated in Feilat et al. (2018).

Moreover, the results of the study carried out in Johnson et al. (2020) indicated that high renewable energy penetrations of more than 80% may be obtainable in the Texas grid, although there are important trade-offs to be considered for such high penetration of non-synchronous generations. In Wiser et al. (2016), the long-term impacts and possible benefits of increasing wind energy penetration in the United States grid was analysed. The authors investigated scenarios of 10%, 20% and 35% wind energy penetration levels for years 2020, 2030 and 2050 respectively and discussed the associated social and economic impacts.

However, there is paucity of studies on the impact of increased renewable energy integration on the power grid of a developing country such as Nigeria. Although, some researchers have analysed the potentials and prospects of large-scale, grid-connected wind power generation in Nigeria (Ajayi, 2010; Ayodele et al., 2016; Shaaban and Petinrin, 2014; Mas'ud et al., 2017; Adedipe et al., 2018; Igbinovia, 2014) and the studies show that Northern Nigeria has enormous wind resource sufficient for wind power generation, much has not been done to effectively harness this resource. At present, the Nigerian economy is essentially dependent on oil and gas. This has made the electricity sector to be primarily driven by fossil fuel. However, shortage of gas supply to the gas thermal stations and vandalization of gas pipelines are precursors of several forced outages. In spite of the good potentials for wind energy generation in Northern Nigeria, there has not been significant progress in harnessing this resource. In response to this, the Nigerian government approved the National Energy Policy in 2003 in order to encourage sustainable harnessing, development and utilization of available and viable renewable energy resources, including wind energy (Adewuyi et al., 2019). Therefore, deliberate policy implementations and investments in wind energy by the Nigerian government will play significant role in meeting the electricity needs of the people and in reducing dependence on oil and gas.

This work therefore assesses the impact of large-scale DFIG-based WECS integration on the voltage stability of weak national grids, with Nigerian power grid as a case study. This present work clearly demonstrates the possibility of utilizing DFIG-based wind energy conversion system (WECS) to mitigate overvoltage occurrence and to improve the voltage stability of weak power grids while meeting the increasing energy demand as seen in the case study analysis of Nigeria in this work. Wind power penetration level (PL) used in this work is the fraction of the real power obtained from the DFIG-based WECS to the total real power from both conventional generators and the WECS. A similar definition was utilized in Eftekharnejad et al. (2013) and (Yu et al., 2016).

The main contributions of this study can be summarized as follows:

- This paper examines the application of utility-scale DFIG-based wind energy conversion system to improve the voltage stability of weak grids.
- A voltage instability tendency measure called critical voltage-reactive power ratio (CVQR) has been derived from QV curve analysis. The performance of this index has been compared with tangent vector derived from PV curve analysis and then utilized to investigate the voltage instability tendency of the wind-connected grid.
- This work also employs megawatt margin obtained from PV curve and the reactive power margin derived from QV curve to evaluate the effects of increased penetration level of DFIG-based wind energy conversion system on the voltage stability of a weak grid. Thus, this work provides a more comprehensive analysis of the steady state voltage stability of wind-connected grid.

The remaining part of the paper is structured as follows: Section 2 provides a background view of the Nigerian 330 kV grid and a brief overview of the wind energy potentials in Nigeria. Modelling of DFIG-based WECS is presented in Section 3 and derivation of tangent vector from PV curve as well as derivation of critical voltage-reactive power ratio are presented in Section 4. Section 5 presents and discusses the results of the voltage stability analysis for different scenarios. This work is summarized and concluded in Section 6.

2. The Nigerian 330 kV power grid

The present status and challenges of the Nigerian power system together with the wind energy potentials in Nigeria are presented in this section.

2.1. Present status and challenges

The expanded 52-bus, 330 kV Nigerian power grid is made up of 18 generators and 65 transmission lines. Fig. 1 shows the single line diagram of the 52-bus system modelled in DIgSILENT PowerFactory. The details of the system parameters are provided in Appendix. According to the final report on the transmission expansion plan in FICHTNER (2017), the gross installed generation capacity is about 13,300 MW. However, statistics from National Control Centre (NCC), Oshogbo, Nigeria indicates that only 5900 MW net capacity has been available. Moreover, the actual daily generation rarely reaches 4000 MW. This is mostly due to several outages, which may be maintenance-based or forced outages. Real peak generation for a typical day is about 3877 MW. In this work, a total base case generation schedule of 3702 MW has been utilized for analysis to correspond with a typical day's generation schedule practically obtainable in the present Nigerian power system.

Some of the challenges of the Nigerian power system includes insufficient generation, erratic power supply, aged power system equipment, high losses and voltage instability issues. The Northern region where there is no large-scale power generation at present is particularly prone to voltage instability. Overvoltage issues exist at the Northern region because of the excessive reactive power build-up along the long transmission line connecting

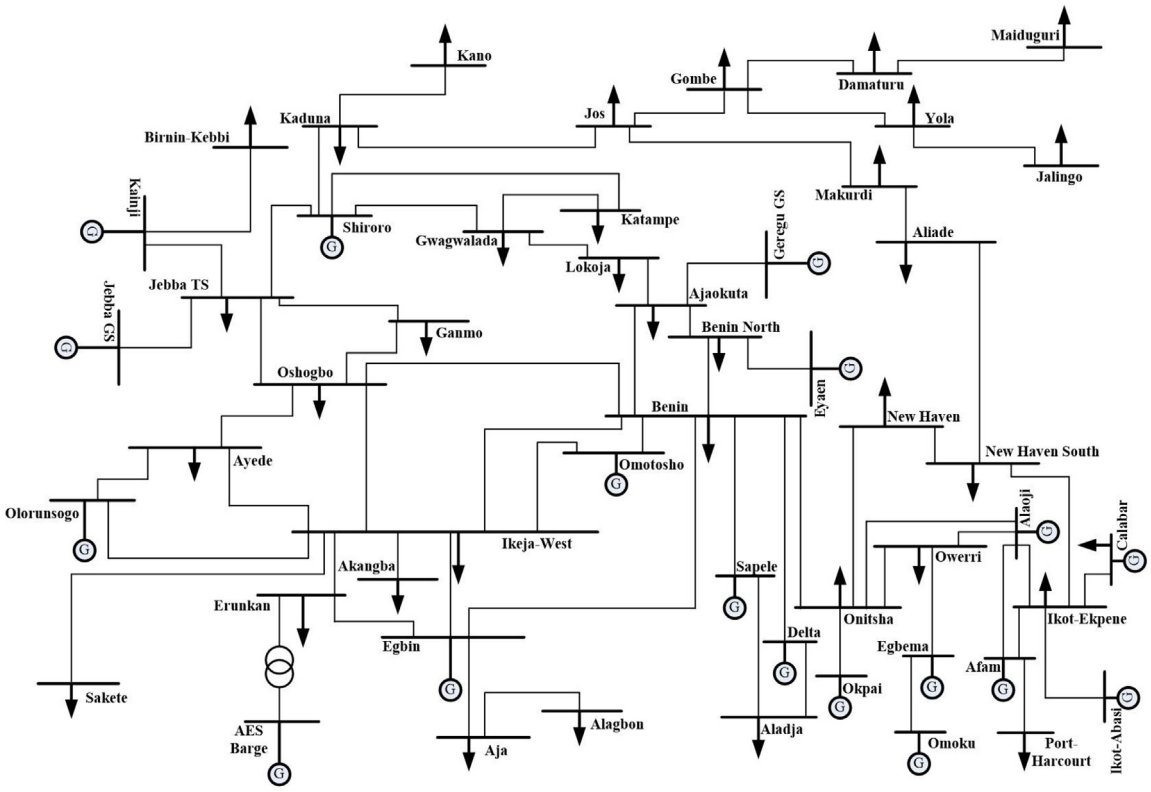

Fig. 1. Single Line Diagram of Nigerian 330 kV Power Grid modelled in DIgSILENT PowerFactory.

the central region to the Northern region (NERC, 2019). Therefore, this necessitates the use of reactive power absorbing devices, which are shunt reactors in some Northern substations in order to absorb the excessive reactive power (FICHTNER, 2017).

Furthermore, the insufficient power generation invariably leads to permanent load shedding within the Nigerian power grid. Also, frequent transmission and distribution system disturbances exacerbate the insecurity of power supply across the country. Thus, there is a need for generation, transmission and distribution expansion of the Nigerian national grid.

At the distribution level, there are eleven Distribution Companies (DisCos) in Nigeria that cover the entire country. Fig. 2 shows the DisCos and the respective states they supply (Nigeria-Electricity-Regulatory-Commission, 2019). The projected total load demand for year 2020 presented by these eleven DisCos in January 2017 sums up to 10282 MW including an export amount of 387 MW (FICHTNER, 2017). However, only a fraction of this total load demand can be supplied by the available generation capacity. The load demand for each DisCos is depicted in Table 1. It can be observed from the table that the load demand is largely in the Southern parts of Nigeria, while the Northern parts are lightly-loaded. In this work, a practical total load demand of 3658 MW has been used. This corresponds to 35.6% of the total load demand. Therefore, the effect of load shedding and limited generation has been considered in this work for practical system analyses.

Power generation is mostly concentrated in the Southern parts of the country, near the oil and gas supplies. It is therefore essential to install new generating plants in the Northern region. However, the major limitation to oil and gas-dependent generation in the Northern parts is the required massive gas pipeline extension from the Niger-Delta region to the Northern region and the occurrence of gas pipeline vandalization. Thus, installation of conventional gas-fired thermal plants in the Northern areas may be quite challenging considering the issue of gas supply.

Table 1
The DisCos load demand for year 2020.

S/N	DisCo	Load demand
1	Abuja	745
2	Benin	1273
3	Eko	1320
4	Enugu	1090
5	Ibadan	1225
6	Ikeja	1250
7	Jos	442
8	Kaduna	590
9	Kano	705
10	Port Harcourt	946
11	Yola	309

Three generating stations closest to the Northern areas are located in the West Central region. These are the Kainji, Shiroro and Jebba Hydro Power Plants. There are also ongoing hydro and thermal plants project such as Kaduna Power Plant, Zungeru Hydro Power Plant, and Kashimbilla HPP. However, the renewable energy potentials such as wind and solar in the northern region are still yet to be considerably harnessed, although there is a 10 MW wind farm at Katsina, which is near completion. Thus, an appropriate generation expansion plan must consider and incorporate renewable energy resources such as wind, which is significantly available in the Northern region.

2.2. Wind energy potentials in Nigeria

Several researchers have investigated the potentials of large-scale wind energy generation and integration to the Nigerian national grid (Ajayi, 2010; Shaaban and Petinrin, 2014; Mas'ud et al., 2017; Adedipe et al., 2018; Igbinovia, 2014). Wind speed profile from Nigerian meteorological Agency based on a 40-year (1968–2007) average wind data from all the forty-four wind

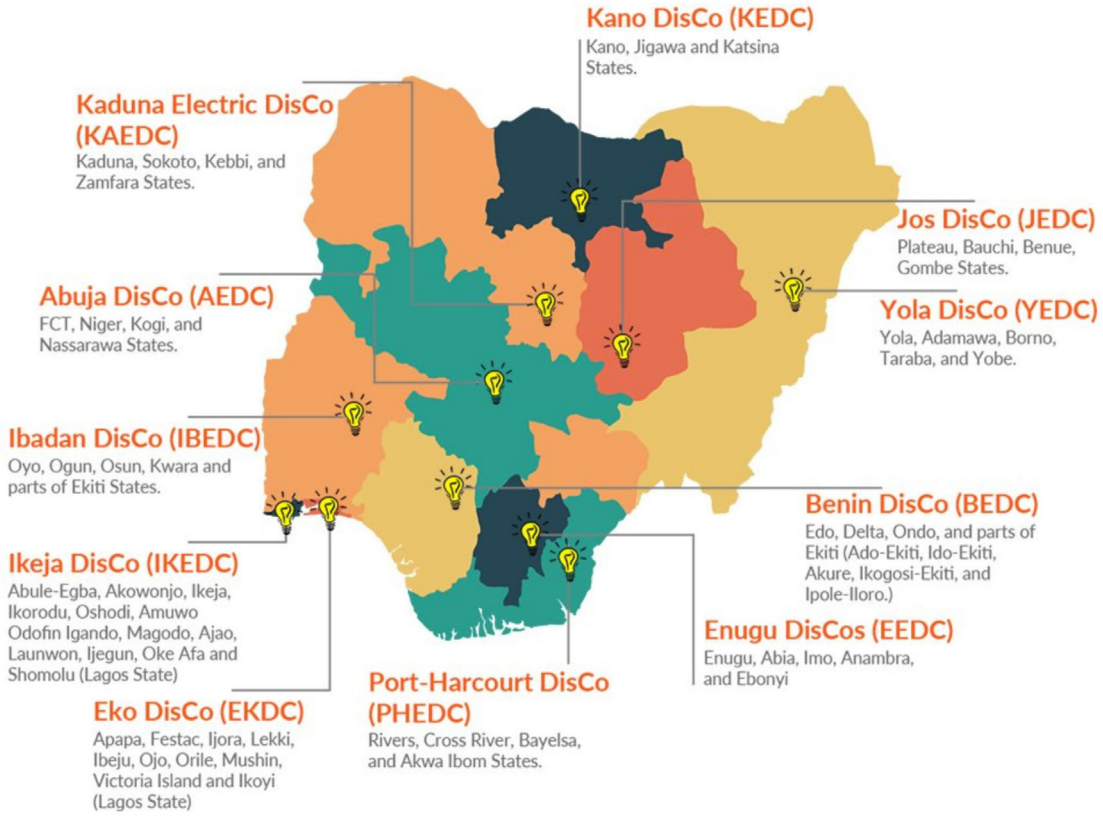

Fig. 2. Map of Nigeria showing the DisCos with their coverage.
Source: Nigerian Electricity Regulatory Commission.

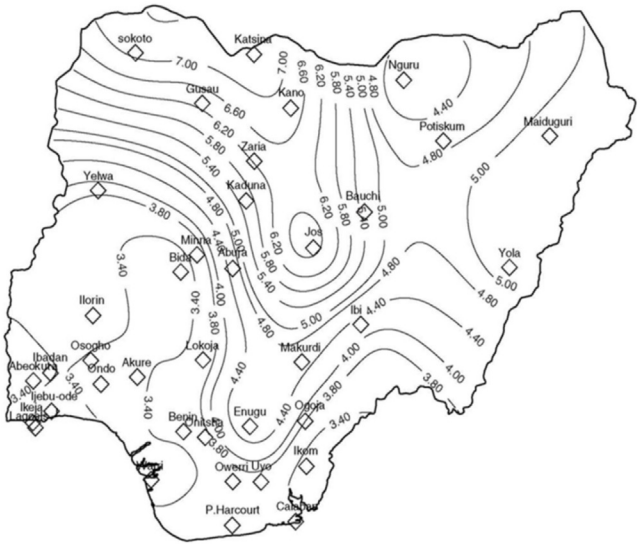

Fig. 3. Map of average wind speed in different parts of Nigeria (Mas'ud et al., 2017).

stations across the country for a nominal height of 10 m indicate that the Nigerian wind speed regime ranges from 3.0–4.4m/s in the Southern parts to about 4.4–7.5m/s in the Northern parts of the country. The map indicating the wind speed regime in Nigeria is shown in Fig. 3. It is clear from the figure and from other indigenous researchers that the Northern parts of the country like Sokoto, Katsina, Kano and Jos have the highest wind energy potentials within the country.

The wind speed regime is generally weak in the Southern parts except at the offshore, coastal region of the country. There is thus an increasing awareness of the possibility of large-scale wind power generation and integration to the national grid. When this wind resource is effectively harnessed, there will be significant progress in addressing the power and energy situation in Nigeria as both off-grid and grid-connected wind energy conversion systems can be put in place to meet the energy needs of locations within the Northern region. Presently, a 10 MW wind farm located in the Northern region of Katsina State is 98% completed. This is the only large-scale wind energy conversion system in Nigeria.

The result of the study on wind energy potentials in 14 Northern states of Nigeria has been reported in Cervigni et al. (2013). The report shows that more than 19 GW of electricity can be generated from all the 14 states by considering only 1% of suitable areas in each state and a capacity factor of 30%. Thus, investments in wind energy generation and integration can play a significant role in mitigating over-dependence on oil and gas for electricity generation and in meeting the increasing electricity demand in the country.

3. DFIG-based WECS modelling

The mechanical output power of a wind turbine can be expressed as (Adetokun et al., 2018):

$$P_t = 0.5 C_p(\lambda, \beta)\, \rho A v_w^3 \tag{1}$$

where C_p is the coefficient of performance of the turbine, λ and β are the tip speed ratio and pitch angle of blade respectively, ρ is the density of air, A is the swept area of the turbine blade

and v_w is the wind speed. The coefficient of performance can be expressed as (Ogunjuyigbe et al., 2016):

$$C_p(\lambda,\beta) = 0.5176\left(\frac{116}{\lambda_1} - 0.4\beta - 5\right)e^{\frac{-21}{\lambda_1}} + 0.0068\lambda$$
$$\lambda_1 = \left[\left(\beta^3+1\right)(\lambda+0.08\beta)\right]\left(\beta^3 - 0.028\beta - 0.035\lambda + 1\right)^{-1} \quad (2)$$

The tip speed ratio is the ratio of the turbine blade linear speed to the wind speed and can be expressed as:

$$\lambda = \frac{\omega_t R_t}{v_w} \quad (3)$$

where ω_t is the tip speed of the turbine rotor blade in rad/s, and R_t is the blade radius. The mechanical torque developed by the wind turbine can be expressed as:

$$T_t = \frac{P_t}{\omega_t} = \frac{0.5C_p(\lambda,\beta)\rho A v_w^3}{\omega_t} \quad (4)$$

The dynamic model of the DFIG in synchronously rotating reference frame can be expressed as (Adetokun et al., 2020a):

$$\begin{aligned} v_{qs} &= -r_s i_{qs} + \omega_e\lambda_{ds} + p\lambda_{qs} \\ v_{ds} &= -r_s i_{ds} - \omega_e\lambda_{qs} + p\lambda_{ds} \\ v'_{qr} &= -r_r i'_{qr} + (\omega_e - \omega_r)\lambda'_{dr} + p\lambda'_{qr} \\ v'_{dr} &= -r_r i'_{dr} - (\omega_e - \omega_r)\lambda'_{qr} + p\lambda'_{dr} \end{aligned} \quad (5)$$

The flux linkage equations are expressed as:

$$\begin{aligned} \lambda_{qs} &= -\left[(L_{ls}+L_M)i_{qs} + L_M i'_{qr}\right] \\ \lambda_{ds} &= -\left[(L_{ls}+L_M)i_{ds} + L_M i'_{dr}\right] \\ \lambda'_{qr} &= -\left[\left(L'_{lr}+L_M\right)i'_{qr} + L_M i_{qs}\right] \\ \lambda'_{dr} &= -\left[\left(L'_{lr}+L_M\right)i'_{dr} + L_M i_{ds}\right] \end{aligned} \quad (6)$$

The real and reactive power of the DFIG stator and rotor circuits can be represented as:

$$\begin{aligned} P_s &= 1.5\left(v_{ds}i_{ds} + v_{qs}i_{qs}\right) \\ Q_s &= 1.5\left(v_{qs}i_{ds} - v_{ds}i_{qs}\right) \\ P_r &= 1.5\left(v'_{dr}i_{dr} + v'_{qr}i'_{qr}\right) \\ Q_r &= 1.5\left(v'_{qr}i'_{dr} - v'_{dr}i'_{qr}\right) \end{aligned} \quad (7)$$

where $v_{qs}(v_{ds})$ is the q-axis (d-axis) stator voltage, $v'_{qr}(v'_{dr})$ is the q-axis (d-axis) rotor voltage, $i_{qs}(i_{ds})$ is the q-axis (d-axis) stator current, $i'_{qr}(i'_{dr})$ is the q-axis (d-axis) rotor current, $\lambda_{qs}(\lambda_{ds})$ is the q-axis (d-axis) stator flux linkage, $\lambda'_{qr}(\lambda'_{dr})$ is the q-axis (d-axis) rotor flux linkage, $r_s(r'_r)$ is the stator (rotor) resistance, L_M is the magnetizing inductance, $L_{ls}(L'_{lr})$ is the stator (rotor) leakage inductance, ω_e is the synchronous speed, ω_r is the rotor speed, ω is the reference frame speed and p is the differential operator.

The DFIG-based WECS used in this work is a variable speed wind turbine generator (Kaloi et al., 2016). Thus, it is able to achieve fast and accurate active power regulation by means of power converter controls and to mitigate the power fluctuations arising from changing wind speed conditions (Wu et al., 2018). Field orientation control is applied to both the grid-side and rotor-side converters to achieve a desirable control of voltage and power. Also, the DFIG-based WECS is equipped with maximum power point tracking such that it is able to extract the maximum power at different wind speeds. The variable-speed capability of DFIG-based WECS enables the generator speed to be controllable within a considerably large range to obtain desired output power through the field orientation control and maximum power point tracking strategies (Zou, 2015). These makes it possible for the DFIG-based WECS to be operated as a generator-controlled bus, with specified active power and bus voltage for steady-state operation of the grid.

4. PV and QV curves based indices

Both PV and QV analyses have been used to carry out the steady-state voltage stability analysis in this work. Since the concepts of PV and QV curves are well established in literature, only their application in determining the critical bus and in assessing the voltage stability of power system have been presented here.

4.1. Tangent Vector (TV) and Active Power Margin (APM)

Tangent Vector (TV) can be computed from PV curve analysis for each power system bus and then utilized to identify the critical bus (CB). The tangent vector is a set of the ratio of differential change in voltage (dV) to differential change in load demand (dP) at each bus. The bus that is associated with the largest gradient (dV/dP) in the final converging iteration-step of the continuation load flow is identified as the critical bus of the system. If the last gradient is positive, which can occur when the load flow solver obtains the wrong solution in the (K-1)th iteration, the cumulative gradient of the bus is checked. If this cumulative gradient from the first to the last iteration ($1{:}K$) of this bus is greater than half that of the bus with the maximum gradient, then the bus with the largest cumulative gradient is considered to be the critical bus, otherwise, the bus with the maximum gradient is the critical bus. Therefore, for an n-bus system, let

$$\begin{aligned} CB' &= \max\left\{\left|\frac{dV_1}{dP}\right|, \left|\frac{dV_2}{dP}\right|, \left|\frac{dV_3}{dP}\right|, \ldots \left|\frac{dV_n}{dP}\right|\right\}^K \\ CB'' &= \max\left\{\sum_{i=1}^K\left|\left(\frac{dV_1}{dP}\right)^i\right|, \sum_{i=1}^K\left|\left(\frac{dV_2}{dP}\right)^i\right|, \right. \\ &\quad \left.\sum_{i=1}^K\left|\left(\frac{dV_3}{dP}\right)^i\right|, \ldots \sum_{i=1}^K\left|\left(\frac{dV_n}{dP}\right)^i\right|\right\} \end{aligned} \quad (8)$$

where the iteration steps are defined as $i = 1{:}K$.

If $\left(\frac{dV}{dP}\right)^K > 0 \& CB'' > \left(CB'/2\right)$, then the critical bus, CB is identified as:

$$CB_{TV} = CB'' = \max\left\{\sum_{i=1}^K\left|\left(\frac{dV_1}{dP}\right)^i\right|, \sum_{i=1}^K\left|\left(\frac{dV_2}{dP}\right)^i\right|, \sum_{i=1}^K\left|\left(\frac{dV_3}{dP}\right)^i\right|, \ldots \sum_{i=1}^K\left|\left(\frac{dV_n}{dP}\right)^i\right|\right\} \quad (9)$$

Otherwise,

$$CB_{TV} = CB' = \max\left\{\left|\frac{dV_1}{dP}\right|, \left|\frac{dV_2}{dP}\right|, \left|\frac{dV_3}{dP}\right|, \ldots \left|\frac{dV_n}{dP}\right|\right\}^K \quad (10)$$

Moreover, the active power margin (APM) also known as the megawatt margin (MWM) is a measure of the system's loadability. It is obtained by subtracting the base load (P_0) from the critical load demand (P_C) obtained from the PV curve and the base case load demand. Thus, the APM is given as:

$$APM = P_C - P_0 \quad (11)$$

4.2. Reactive power margin and critical voltage-reactive power ratio

The Reactive Power Margin (RPM) and Critical Voltage-Reactive Power Ratio (CVQR) index are derived from QV curves for each bus of the power system. This approach can also be used to identify the critical bus and to obtain insights concerning the voltage stability status of the system. The reactive power margin denotes the maximum reactive power that can be absorbed from a bus. When this value is exceeded, the system experiences voltage collapse. The corresponding voltage at which this reactive power is reached is the critical voltage. CVQR is the ratio of the critical voltage to the critical reactive power in p.u. The critical

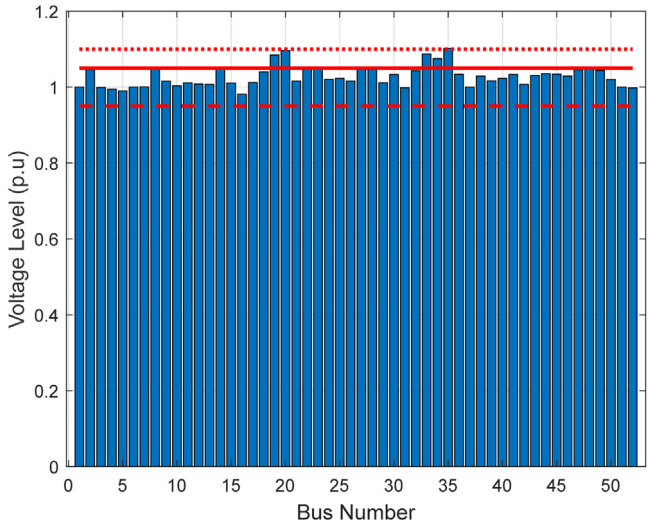

Fig. 4. Voltage Profile of the 52-bus Nigerian 330 kV Power Grid.

reactive power is negative for normal operating conditions and positive when voltage collapse occurs. Therefore, CVQR index associated with all the system buses are negative for normal operating conditions. Thus, when all the CVQR values of an n-bus power system are negative, the critical bus can be identified as:

$$CB_{CVQR} = \min\left\{\frac{V_{c1}}{Q_{c1}}, \frac{V_{c2}}{Q_{c2}}, \frac{V_{c3}}{Q_{c3}}, \ldots \frac{V_{cn}}{Q_{cn}}\right\} \tag{12}$$

If the CVQR index of any bus is positive, this indicates a condition of voltage collapse. Thus, the RPM and the CVQR are utilized to assess the effects of increased wind power PL on the steady-state voltage stability of the system under study. The accuracy of the CVQR has been verified by comparing its bus ranking performance to that obtained from the tangent vector and RPM.

5. Results and discussion

The results of the voltage stability analysis are presented and discussed in this section. Three cases have been investigated. All simulations have been done using DIgSILENT PowerFactory. However, the results are imported into MATLAB to generate the plots of the results since MATLAB plotting functions are more flexible to use.

5.1. Case one: Base case scenario

First, we present the voltage profile of the buses as obtained from the load flow analysis of the system. The voltage profile is depicted in Fig. 4. It can be observed that the voltage levels at bus 19 (Gombe), bus 20 (Yola), bus 33 (Damaturu), bus 34 (Maiduguri) and bus 35 (Jalingo) exceeds 1.05 p.u. This is in confirmation of the overvoltage issues presently being experienced in Northern Nigeria. The overvoltage problem results from the reactive power build up along the long transmission lines connecting the central parts to the Northern parts of Nigeria. In addition, these buses are lightly loaded. This is why shunt reactors are presently employed in the Nigerian power system. The shunt reactors absorb the excess reactive power in order to maintain an acceptable voltage level. When shunt reactors are applied at Gombe, Kaduna, kano, Yola and Maiduguri, only the Jalingo bus voltage level reaches 1.10p.u as indicated in the figure. It can also be noted that none of the bus voltage levels fall below the acceptable level of 0.95 p.u.

The PV curve for selected Northern buses are depicted in Fig. 5. The figure indicates that the maximum scalable load demand is 5028 MW for a base case demand of 3658 MW and the tangent vector of the buses obtained from the PV curve analysis indicates that the Jalingo bus is the critical bus of the system.

Moreover, the QV curve analysis indicates that the least reactive power margin of the system is 139.6MVAR, which is the value recorded for the Jalingo bus. In addition, the Jalingo bus has the most negative CVQR index value of −0.4586. This indicates that Jalingo bus is the critical bus in the 52-bus Nigerian 330 kV Power Grid. The determination of Jalingo bus as the critical bus in this work is similar to the result obtained in Akwukwaegbu et al. (2017), which also identifies Jalingo bus as the weakest bus in the 52-bus Nigerian power system using eigenvalue method.

The ranking of the first ten critical buses using the PV and QV-based approaches are shown in Table 2. Bus ranking based on tangent vector (TV), RPM and CVQR index are compared in the table. The comparison shows that Jalingo, Yola, Maiduguri, Damaturu, and Gombe are the five weakest buses. Although there

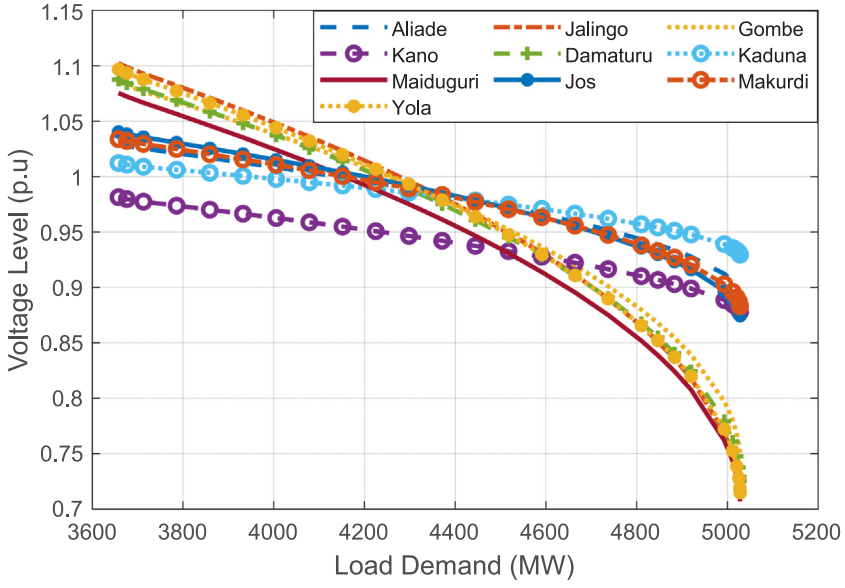

Fig. 5. PV Curves for Selected Northern Buses.

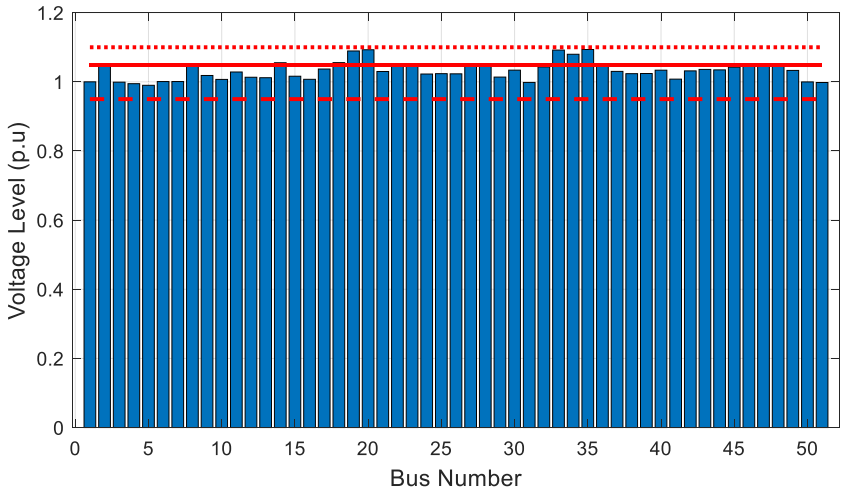

Fig. 6. Voltage Profile of Nigerian 330 kV Power Grid for Case 2.

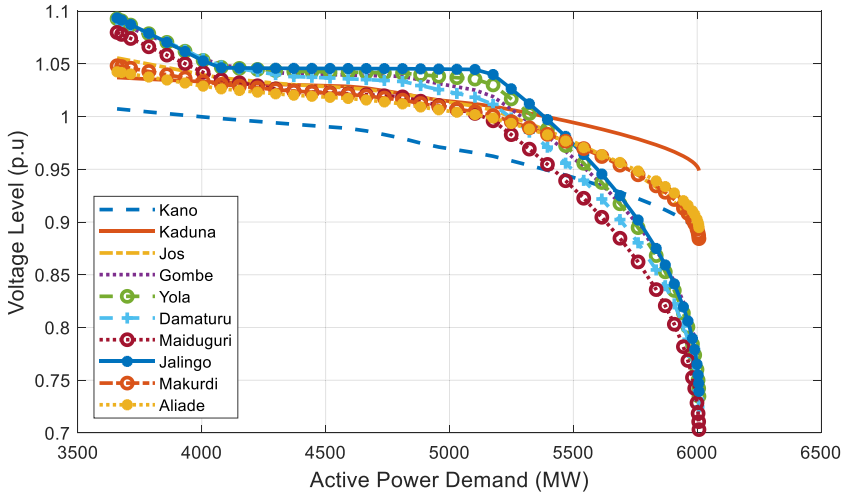

Fig. 7. PV Curves of Selected Northern Buses Case 2.

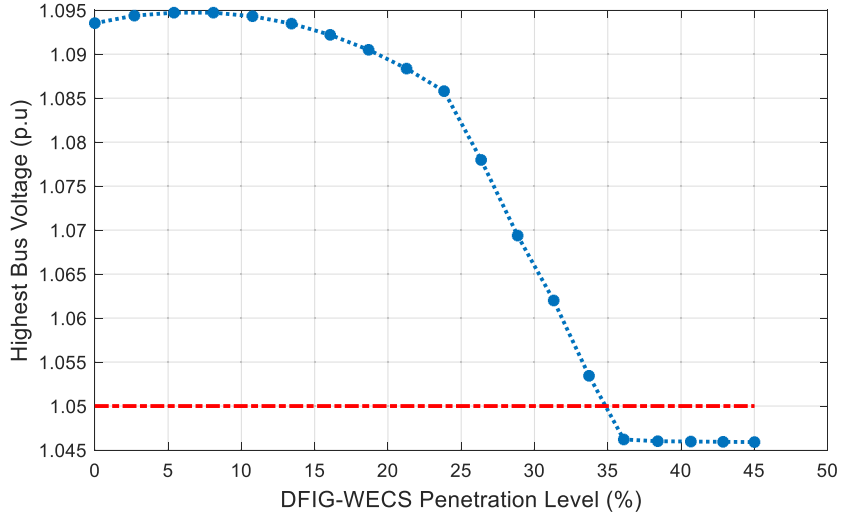

Fig. 8. Variation of Highest Bus Voltage with DFIG –WECS Penetration Level.

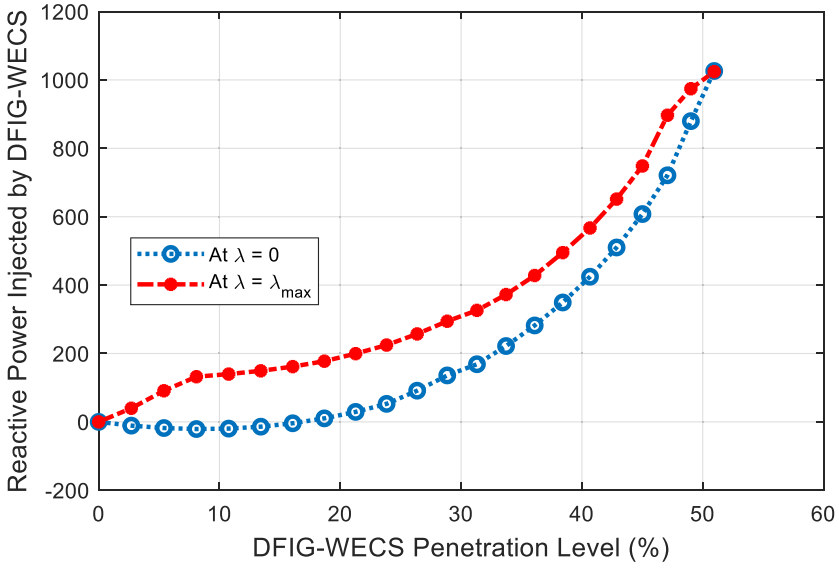

Fig. 9. Reactive Power Injected by the DFIG-based WECS.

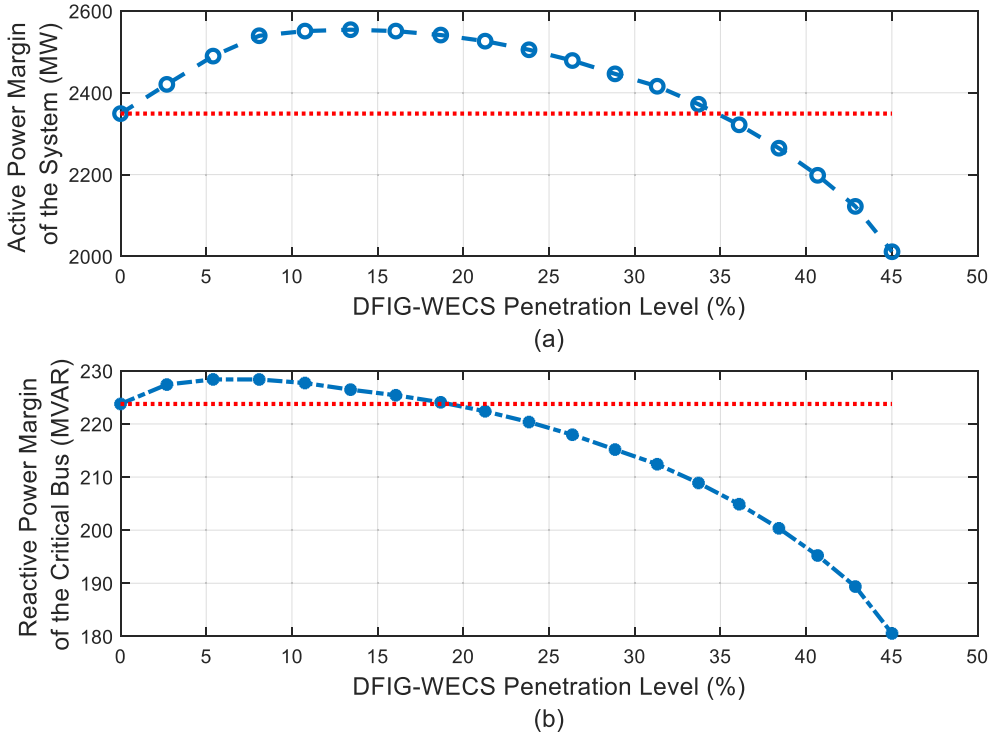

Fig. 10. Variation of Active and Reactive Power Margins with DFIG-based WECS PL.

are slight variations in the rankings, the results invariably depict that the northern buses constitute the weakest buses in the Nigerian Power Grid.

5.2. Case two: Incorporation of nearly-completed generation systems

In this section, the static voltage stability of the Nigerian 330 kV Power Grid is carried out when new conventional generation systems are incorporated into the grid. New generation systems that are near to completion includes the following:

- 200 MW Kaduna and 30 MW Gurara Power Plants, Kaduna State
- 29 MW Dadin-Kowa Hydro Power Station, Gombe State
- 40 MW Kashimbilla Hydro Power Plant, Taraba State

The load flow analysis for this case shows that some of the bus voltage profiles still exceed the recommended upper limit of 1.05p.u although the highest voltage level is 1.0935p.u as recorded for bus 35 (Jalingo bus). This is better when compared with the base case scenario. The complete voltage profile is depicted in Fig. 6. None of the bus voltage level falls below 0.95p.u as observed from the figure.

Fig. 7 shows the PV curve for selected Northern buses for this case. It can be observed that the maximum scalable demand, which is an indication of the system's loadability has improved

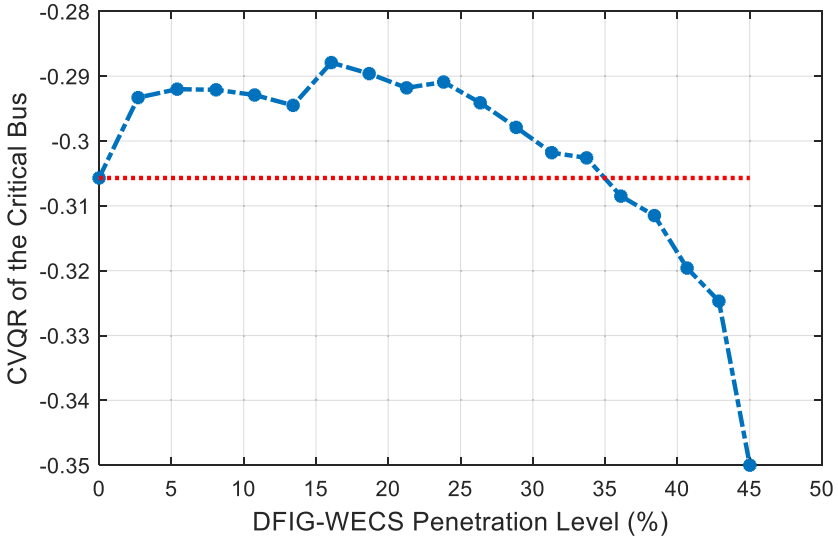

Fig. 11. Variation of Critical Bus CVQR with Increasing DFIG-based WECS PL.

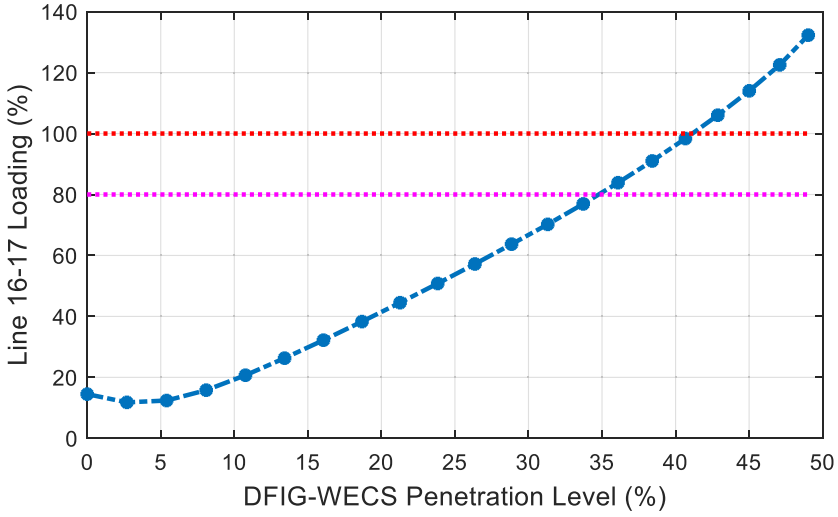

Fig. 12. Variation of Line 16–17 Loading with DFIG-based WECS PL.

Table 2
Bus ranking comparison of the Nigerian 330 kV Power Grid.

Rank	Bus	TV	Bus	RPM	Bus	CVQR
1	Jalingo	0.7266	Jalingo	139.57	Jalingo	−0.4586
2	Yola	0.7065	Maiduguri	152.83	Yola	−0.4286
3	Maiduguri	0.6755	Yola	153.99	Maiduguri	−0.4122
4	Damaturu	0.6636	Damaturu	172.16	Damaturu	−0.3892
5	Gombe	0.6171	Gombe	201.7	Gombe	−0.3471
6	Jos	0.2687	Kano	403.3	Jos	−0.1439
7	Makurdi	0.2407	Birnin-Kebbi	451.23	Kano	−0.1438
8	Aliade	0.2114	Jos	528.26	Makurdi	−0.1296
9	Kano	0.1207	Makurdi	578.78	Birnin-Kebbi	−0.1285
10	Kaduna	0.1104	Aliade	648.84	Aliade	−0.1140

from the base case value of 5028 MW maximum scalable demand to 6007.1 MW. This shows that with the incorporation of the nearly-completed conventional generation systems, the system's loadability is enhanced, with an additional megawatt (active power) margin of 979.1 MW. In addition, the RPM of the most critical bus increases from the base case value of 139.57MVAR to 223.77MVAR. Thus, with the new conventional generation systems concentrated in the Northern region and totalling 299 MW, the loadability margins and voltage stability of the system are enhanced as indicated by the increase in both the active and reactive power margins of the system.

5.3. Case three: Large-scale DFIG-based WECS integration in northern region

The static voltage stability of the Nigerian 330 kV grid with large-scale DFIG-based WECS integration is analysed in this section. DFIG-based WECS is located in Katsina, Northern Nigeria, where the 10 MW wind farm is sited. The large-scale integration of DFIG-based WECS is investigated for penetration levels (PLs) ranging from 100 MW (2.7% PL) to 1800 MW (45% PL). The effects of the increased DFIG-based WECS PL on the bus voltage profile is performed using load flow analysis. Also, the impact of this increased PL on voltage stability margins of the wind-integrated grid are evaluated using PV and QV curves analyses. The PV curve provides the total active power margin (APM) of the system while the QV analysis gives the Reactive Power Margin (RPM) and the associated CVQR of the system for each PL scenario.

Fig. 8 depicts the impact of increased DFIG-based WECS integration on the variation of the highest bus voltage in the system,

Table A.1
Line data of the 52-bus 330 kV Nigerian Power Grid.

S/N	Line	Name	L km	Line type	R1 (Ω/km)	X1 (Ω/km)	B1 (μS/km)	R0 (Ω/km)	X0 (Ω/km)	B0 (μS/km)
1	01—02	Egbin-Benin	218	SC × 1	0.039	0.331	3.49	0.276	0.985	2.49
2	01—03	Egbin-Ikeja West	62	DC × 2	0.038642	0.30211	3.806392	0.27225	0.995908	2.280873
3	01—31	Egbin-Aja	14	DC × 2	0.0394	0.303	3.812	0.274	0.997	2.295
4	01—51	Egbin-Erunkan	30	SC × 1	0.039	0.331	3.49	0.276	0.985	2.49
5	02—03	Benin-Ikeja West	280	DC × 2	0.038893	0.302975	3.810836	0.274195	0.995657	2.295684
6	02—08	Benin-Omotoso	51	SC × 1	0.039	0.331	3.49	0.276	0.985	2.49
7	02—09	Benin-Osogbo	251	SC × 1	0.038614	0.331039	3.490172	0.275938	0.984873	2.487753
8	02—22	Benin-Ajaokuta	195	SC × 2	0.039092	0.312738	3.508276	0.273646	0.988477	2.50053
9	02—24	Benin-Onitsha	137	SC × 2	0.039	0.331	3.49	0.276	0.985	2.49
10	02—27	Benin-Sapele	50	DC × 2	0.039204	0.302742	3.820018	0.274428	0.997524	2.295684
11	02—28	Benin-Delta	41	SC × 1	0.039	0.331	3.49	0.276	0.985	2.49
12	02—48	Benin-Benin North	20	SC × 3	0.039	0.331	3.49	0.276	0.985	2.49
13	03—04	Ikeja West-Akangba	17	SC × 2	0.039	0.331	3.49	0.276	0.985	2.49
14	03—05	Ikeja West-Sakete	70	SC × 1	0.039	0.331	3.49	0.276	0.985	2.49
15	03—06	Ikeja West-Ayede	137	SC × 1	0.039	0.331	3.49	0.276	0.985	2.49
16	03—07	Ikeja West-Papalanto	30	SC × 1	0.039	0.331	3.49	0.276	0.985	2.49
17	03—08	Ikeja West-Omotoso	200	SC × 1	0.039	0.331	3.49	0.276	0.985	2.49
18	03—09	Ikeja West-Osogbo	250	SC × 1	0.039	0.331	3.49	0.276	0.985	2.49
19	03—51	Ikeja West-Erunkan	32	SC × 1	0.039	0.331	3.49	0.276	0.985	2.49
20	06—07	Ayede-Papalanto	60	SC × 1	0.039	0.331	3.49	0.276	0.985	2.49
21	06—09	Ayede-Osogbo	115	SC × 1	0.038825	0.330488	3.48944	0.275564	0.984835	2.491316
22	09—10	Osogbo-Ganmo	75	SC × 1	0.039	0.331	3.49	0.276	0.985	2.49
23	09—12	Osogbo-Jebba TS	157	SC × 3	0.038843	0.330862	3.491779	0.276065	0.984955	2.491621
24	10—12	Ganmo-Jebba TS	80	SC × 1	0.039	0.331	3.49	0.276	0.985	2.49
25	11—12	Shiroro-Jebba TS	244	SC × 2	0.039	0.331	3.49	0.276	0.985	2.49
26	11—17	Shiroro-Kaduna	96	SC × 2	0.038569	0.331238	3.481788	0.277922	0.984638	2.486991
27	11—21	Shiroro-Katampe	144	DC × 2	0.0394	0.303	3.812	0.274	0.997	2.295
28	11—50	Shiroro-Gwagwalada	114	DC × 2	0.0394	0.303	3.812	0.274	0.997	2.295
29	12—13	Jebba GS-Jebba TS	8	DC × 2	0.040838	0.299475	3.810836	0.27225	0.993713	2.295684
30	12—15	Kainji-Jebba TS	81	SC × 2	0.038989	0.330733	3.491707	0.275611	0.985478	2.494077
31	14—15	Birnin Kebbi- Kainji	310	SC × 2	0.038993	0.330915	3.48944	0.276114	0.983613	2.488225
32	16—17	Kaduna-Kano	230	SC × 2	0.039	0.331	3.49	0.276	0.985	2.49
33	17—18	Kaduna-Jos	196	SC × 2	0.038695	0.331122	3.486643	0.270868	0.98397	2.489128
34	18—19	Jos-Gombe	264	SC × 2	0.03904	0.332864	3.499835	0.275332	0.986264	2.491467
35	18—36	Makurdi-Jos	230	DC × 2	0.0394	0.303	3.812	0.274	0.997	2.295
36	19—20	Gombe-Yola	240	SC × 2	0.039	0.331	3.49	0.276	0.985	2.49
37	19—33	Gombe-Damaturu	135	SC × 1	0.039	0.331	3.49	0.276	0.985	2.49
38	20—35	Yola-Jalingo	132	SC × 1	0.039	0.331	3.49	0.276	0.985	2.49
39	21—50	Gwagwalada-Katampe	30	DC × 2	0.0394	0.303	3.812	0.274	0.997	2.295
40	22—23	Ajaokuta-Geregu	1	DC × 2	0.0394	0.303	3.812	0.274	0.997	2.295
41	22—48	Benin North-Ajaokuta	195	SC × 2	0.039	0.331	3.49	0.276	0.985	2.49
42	22—49	Ajaokuta-Lokoja	38	DC × 2	0.0394	0.303	3.812	0.274	0.997	2.295
43	24—25	Alaoji-Onitsha	138	SC × 1	0.038667	0.330646	3.486778	0.276196	0.986413	2.488655
44	24—26	New Haven-Onitsha	96	SC × 1	0.038569	0.331238	3.491353	0.27225	0.984638	2.486991
45	24—29	Onitsha-Okpai	60	DC × 2	0.0394	0.303	3.812	0.274	0.997	2.295
46	24—38	Owerri-Onitsha	137	DC × 2	0.0394	0.303	3.812	0.274	0.997	2.295
47	25—30	Alaoji-Afam	25	DC × 2	0.0394	0.303	3.812	0.274	0.997	2.295
48	25—38	Owerri-Alaoji	60	DC × 2	0.0394	0.303	3.812	0.274	0.997	2.295
49	25—40	Alaoji-Ikot Ekpene	38	DC × 2	0.0394	0.303	3.812	0.274	0.997	2.295
50	26—39	New Haven-New Haven South	5	DC × 2	0.0394	0.303	3.812	0.274	0.997	2.295
51	27—32	Sapele-Aladja	63	SC × 1	0.039757	0.328429	3.48361	0.276571	0.985286	2.492457
52	28—32	Delta-Aladja	32	SC × 1	0.039	0.331	3.49	0.276	0.985	2.49
53	30—40	Afam-Ikot Ekpene	90	DC × 2	0.0394	0.303	3.812	0.274	0.997	2.295
54	30—41	Afam-Port Harcourt	45	DC × 2	0.0394	0.303	3.812	0.274	0.997	2.295
55	31—52	Aja-Alagbon	26	DC × 2	0.0394	0.303	3.812	0.274	0.997	2.295
56	33—34	Damaturu-Maiduguri	140	SC × 1	0.039	0.331	3.49	0.276	0.985	2.49
57	36—46	Aliade-Makurdi	50	DC × 2	0.0394	0.303	3.812	0.274	0.997	2.295
58	38—45	Owerri-Egbema	30	DC × 2	0.0394	0.303	3.812	0.274	0.997	2.295
59	39—40	Ikot Ekpene-New Haven South	143	DC × 2	0.0394	0.303	3.812	0.274	0.997	2.295
60	39—46	New Haven South-Aliade	150	DC × 2	0.0394	0.303	3.812	0.274	0.997	2.295
61	40—42	Ikot Ekpene-Calabar	72	DC × 2	0.0394	0.303	3.812	0.274	0.997	2.295
62	40—43	Ikot Abasi-Ikot Ekpene	75	DC × 2	0.0394	0.303	3.812	0.274	0.997	2.295
63	44—45	Omoku-Egbema	30	DC × 2	0.0394	0.303	3.812	0.274	0.997	2.295
64	47—48	Eyaen-Benin North	5	DC × 2	0.0394	0.303	3.812	0.274	0.997	2.295
65	49—50	Lokoja-Gwagwalada	140	DC × 2	0.0394	0.303	3.812	0.274	0.997	2.295

which is the Jalingo bus. This is the bus with the highest voltage level, which exceeds the recommended maximum limit of 1.05 p.u. The figure shows that the highest bus voltage initially increases with DFIG-based WECS PL, but begins to reduce and approach the recommended upper limit of 1.05p.u as the PL increases beyond 8.1% PL (300 MW). At about 35% PL (about 1350 MW), the highest bus voltage in the network falls within the acceptable limit.

The reactive power support provided by the DFIG-based WECS is illustrated in Fig. 9. The figure depicts the reactive power injected by DFIG-based WECS as the PL increases both at normal loading conditions ($\lambda = 0$), and at maximum loading point ($\lambda = \lambda_{max}$). The loop formed by the two curves indicates the region within which the DFIG-based WECS is able to generate reactive power for voltage support when the loading of the system increases. The two curves terminate at about 51% PL (2100 MW).

Table A.2
Load data of the 52-bus 330 kV Nigerian Power Grid.

Load	MW	MVAR	Load	MW	MVAR	Load	MW	MVAR
Load 02	188	91	Load 19	113	55	Load 36	60	30
Load 03	321	155	Load 20	71	34	Load 38	12	6
Load 04	297	144	Load 21	189	62	Load 39	60	30
Load 05	91	44	Load 22	60	29	Load 40	15	7
Load 06	170	82	Load 24	102	48	Load 41	10	6
Load 09	148	72	Load 25	167	78	Load 46	50	20
Load 10	170	82	Load 26	140	64	Load 48	18	8
Load 12	260	125	Load 31	139	65	Load 49	16	7
Load 14	71	34	Load 32	105	51	Load 50	10	4
Load 16	157	76	Load 33	60	40	Load 51	14	6
Load 17	173	84	Load 34	50	30	Load 52	17	8
Load 18	89	43	Load 35	45	25	Total	3658	1745

Beyond this point, no additional reactive power can be provided by the DFIG-based WECS at maximum loading point. Thus, this point indicate the overall possible maximum limit for increasing DFIG-based WECS PL for the system under study, even though this point may not be reached because of practical system constraints.

Furthermore, Fig. 10(a) and (b) illustrates the variation of the active power margin (APM) of the system and the RPM of the critical bus with increasing DFIG-based WECS PL. The APM of the system initially improves as the penetration of DFIG-based WECS increases, but begins to decline after 13.4% PL (500 MW). The APM declines to the original base case value at about 35% PL. This exactly corresponds to the PL when the highest bus voltage level comes within the acceptable limit of 1.0 ± 0.05p.u as earlier illustrated in Fig. 8. The RPM of the critical bus, which is the overall minimum RPM of the system exhibits similar behaviour. However, the RPM begins to decline after 8.1% PL and reaches the original base case value at 18.7% PL.

Although, both the APM and the RPM of the system declines as the PL increases, Fig. 11 indicates that the system's static voltage stability is guaranteed nonetheless, since the CVQR of the critical bus remains negative at all investigated PLs. The CVQR index also shows that the voltage stability of the system is better enhanced compared to the base case value as the PL increases. However, the CVQR also returns to its base case value at about 35% PL, after which it begins to become more negative, thereby indicating that the system is tending towards voltage instability after 35% PL.

As an indication of the need for system development when increase in DFIG-based WECS integration is contemplated, some power system elements become overloaded as the PL of DFIG-based WECS increases. Line 16–17 is the most critical system element and its loading with increased DFIG-based WECS PL is shown in Fig. 12. This transmission line connects Kano bus with the Kaduna bus. The figure indicates that this line becomes 80% loaded at about 35% PL. The loading of the line exceeds 100% at about 41.14% PL. Thus, 41.14% is the maximum permissible PL that will not result in overloaded system. Therefore, there is a need for power system equipment upgrade with increasing DFIG-based WECS PL.

From the highest bus voltage profile, APM, CVQR, and Line 16–17 loading characteristics shown in Fig. 8, 10a, 11 and 12 respectively, it can be concluded that the optimal DFIG-based WECS PL is 35%.

6. Conclusion

The impact of integrating large-scale DFIG-based WECS on the voltage stability of the 52-bus, 330 kV Nigerian power grid has been assessed and discussed in this work. PV curve method was used to obtain the maximum loadability of the system while QV curve method was employed to assess the reactive power margin of the system for each investigated penetration level scenario. In addition, the voltage stability status of the wind-integrated system has been assessed using CVQR index. The results indicate that the optimal DFIG-based WECS PL, which satisfies the bus voltage requirement of 1.0 ± 0.05p.u, without the active power margin and CVQR falling below their respective base case values and the loading of the most critical power system equipment not exceeding 80% is 35%. This work has thus illustrated the effectiveness of large-scale DFIG-based WECS integration in improving the voltage profile of the system, thereby mitigating the overvoltage occurrences in the Northern region by ensuring that all bus voltages are within the acceptable limits. Therefore, the wind energy potentials in Northern Nigeria can be harnessed for large-scale wind power generation in order to address the voltage stability issue and to meet the increasing energy demand of the country. The impact of change in wind speed and reactive and active power injection during faults can be investigated in a future study.

CRediT authorship contribution statement

Bukola Babatunde Adetokun: Conceptualization, Methodology, Software, Formal analysis, Writing - original draft, Writing - review & editing. **Christopher Maina Muriithi:** Conceptualization, Methodology, Project Administration, Supervision, Writing - review & editing.

Declaration of competing interest

The authors declare that they have no known competing financial interests or personal relationships that could have appeared to influence the work reported in this paper.

Acknowledgement

This work has been funded by African Union Commission on the platform of Pan African University Scholarship.

Appendix

Table A.1 shows the line parameters of the Nigerian power grid. The line length (L), positive sequence resistance (R1), positive sequence reactance (X1) and positive sequence susceptance (B1) are shown in the table for each line. In addition, the corresponding zero sequence parameters: resistance (R0), reactance (X0), and susceptance (B0) have been indicated.

The load data used for the analysis in this work is provided in Table A.2.

Table A.3 provides the details of the generators in the 52-bus Nigerian power grid. P_{sch} is the scheduled active power of each generator and they correspond to a typical day's generation schedule for the Nigerian power grid as obtained from (FICHTNER, 2017).

Table A.3
Generator data of the 52-bus 330 kV Nigerian Power Grid.

Generators	Plant type	Psch. (MW)	Max. Active Power Limit (MW)	Nominal Apparent Power (MVA)	Min. Reactive Power Limit (MVAR)	Max. Reactive Power Limit (MVAR)
Gen 01_Egbin (Slack Bus)	Steam and Gas	–	1320	1661.4	–	–
Gen 07_Papalanto	Gas	140	335	418.75	−120.0	184.0
Gen 08_Omotosho	Gas	220	335	418.75	−120.0	184.0
Gen 11_Shiroro	Hydro	450	600	706	−260.0	316.0
Gen 13_Jebba	Hydro	475	607	714	−180.0	284.4
Gen 15_Kainji	Hydro	313	760	800	−240.0	246.8
Gen 23_Geregu	Gas	145	444	522	−135.0	255.0
Gen 25_Alaoji	Gas	115	480.25	565	−339.0	395.5
Gen 27_Sapele	Gas	173	1080	1200	−300.0	523.0
Gen 28_Delta	Gas	320	960	1200	−288.0	504.0
Gen 29_Okpai	Gas	423	450	530	−150.0	238.8
Gen 30_Afam	Gas	302	727	910	−390.0	648.0
Gen 37_AES Barge	Gas	0	280	350	−105.0	245.0
Gen 42_Calabar	Gas	120	565	706.25	−423.8	494.4
Gen 43_Ikot-Abasi	Gas	0	196	245	−147.0	171.5
Gen 44_Omoku	Gas	75	150	187.5	−112.5	131.3
Gen 45_Egbema	Gas	0	340	425	−255.0	297.5
Gen 47_Eyaen	Gas	107	452	565	−339.0	395.5

References

Adedipe, O., Abolarin, M.S., Mamman, R.O., 2018. A review of onshore and offshore wind energy potential in Nigeria. In: IOP Conference Series: Materials Science and Engineering. Vol. 413, 012039.

Adetokun, B.B., Adekitan, A.I., Somefun, T.E., Aligbe, A., Ogunjuyigbe, A.S.O., 2018. Artificial neural network-based capacitance prediction model for optimal voltage control of stand-alone wind-driven self-excited reluctance generator. In: 2018 IEEE PES/IAS PowerAfrica. pp. 485–490.

Adetokun, B.B., Muriithi, C.M., Ojo, J.O., 2020a. Voltage stability assessment and enhancement of power grid with increasing wind energy penetration. Int. J. Electr. Power Energy Syst. 120, 105988.

Adetokun, B.B., Muriithi, C.M., Ojo, J.O., 2020b. Voltage stability analysis and improvement of power system with increased SCIG-based wind system integration. In: 2020 IEEE PES/IAS PowerAfrica. pp. 1–5.

Adewuyi, O.B., Shigenobu, R., Senjyu, T., Lotfy, M.E., Howlader, A.M., 2019. Multiobjective mix generation planning considering utility-scale solar PV system and voltage stability: Nigerian case study. Electr. Power Syst. Res. 168, 269–282.

Ahmad, T., Zhang, H., Yan, B., 2020. A review on renewable energy and electricity requirement forecasting models for smart grid and buildings. Sustainable Cities Soc. 55, 102052.

Ajayi, O., 2010. The potential for wind energy in Nigeria. Wind Eng. 34, 303–311.

Akwukwaegbu, I.O., Nosiri, O.C., Ezugwu, E.O., 2017. Voltage stability investigation of the Nigeria 330kv interconnected grid system using eigenvalues method. Am. J. Eng. Res. 6 (4), 168–182.

Astiaso Garcia, D., Bruschi, D., 2016. A risk assessment tool for improving safety standards and emergency management in Italian onshore wind farms. Sustain. Energy Technol. Assess. 18, 48–58.

Ayodele, T.R., Ogunjuyigbe, A.S.O., Adetokun, B.B., 2017. Optimal capacitance selection for a wind-driven self-excited reluctance generator under varying wind speed and load conditions. Appl. Energy 190, 339–353.

Ayodele, T.R., Ogunjuyigbe, A.S.O., Amusan, T.O., 2016. Wind power utilization assessment and economic analysis of wind turbines across fifteen locations in the six geographical zones of Nigeria. J. Cleaner Prod. 129, 341–349.

Bayer, B., Marian, A., 2020. Innovative measures for integrating renewable energy in the German medium-voltage grids. Energy Rep. 6, 336–342.

Bennouk, A., Nejmi, A., Ramzi, M., 2018. Stability enhancement of a wind plant based on a DFIG and a PMSM: A Lyapunov approach. Energy Rep. 4, 13–22.

Bian, X., Geng, Y., Yuan, F., Lo, K.L., Fu, Y., 2016. Identification and improvement of probabilistic voltage instability modes of power system with wind power integration. Electr. Power Syst. Res. 140, 162–172.

Carvajal-Romo, G., Valderrama-Mendoza, M., Rodríguez-Urrego, D., Rodríguez-Urrego, L., 2019. Assessment of solar and wind energy potential in La Guajira, Colombia: Current status, and future prospects. Sustain. Energy Technol. Assess. 36, 100531.

Cervigni, R., Dvorak, I., Rogers, J.A., 2013. Assessing Low-Carbon Development in Nigeria: An Analysis of Four Sectors, in World Bank Studies. The World Bank.

Chen, L., Min, Y., Dai, Y., Wang, M., 2017. Stability mechanism and emergency control of power system with wind power integration. IET Renew. Power Gener. 11 (1), 3–9.

Ciupăgeanu, D.-A., Lăzăroiu, G., Barelli, L., 2019. Wind energy integration: Variability analysis and power system impact assessment. Energy 185, 1183–1196.

da Costa, J.N., Passos Filho, J.A., Mota Henriques, R., 2019. Loading margin sensitivity analysis in systems with significant wind power generation penetration. Electr. Power Syst. Res. 175, 105900.

Eftekharnejad, S., Vittal, V., Heydt, G.T., Keel, B., Loehr, J., 2013. Small signal stability assessment of power systems with increased penetration of photovoltaic generation: A case study. IEEE Trans. Sustain. Energy 4 (4), 960–967.

Esteban, M., et al., 2018. 100% renewable energy system in Japan: Smoothening and ancillary services. Appl. Energy 224, 698–707.

Feilat, E.A., Azzam, S., Al-Salaymeh, A., 2018. Impact of large PV and wind power plants on voltage and frequency stability of Jordan's national grid. Sustainable Cities Soc. 36, 257–271.

FICHTNER, 2017. Transmission expansion plan development of power system master plan for the transmission company of Nigeria. 8328P01/FICHT-19579512-v 1.

Heetun, K.Z., Abdel Aleem, S.H.E., Zobaa, A.F., 2016. Voltage stability analysis of grid-connected wind farms with FACTS: Static and dynamic analysis. Energy Policy Res. 3 (1), 1–12.

Igbinovia, F., 2014. An overview of renewable energy potentials in Nigeria: Prospects, challenges and the way forward. Energetika J. (ISSN: 0375-8842) Index 46 507, 570–579.

Jacobson, M.Z., et al., 2018. 100% clean and renewable Wind, Water, and Sunlight (WWS) all-sector energy roadmaps for 53 towns and cities in North America. Sustainable Cities Soc. 42, 22–37.

Jadidbonab, M., Vahid-Pakdel, M.J., Seyedi, H., Mohammadi-ivatloo, B., 2019. Stochastic assessment and enhancement of voltage stability in multi carrier energy systems considering wind power. Int. J. Electr. Power Energy Syst. 106, 572–584.

Johnson, S.C., Rhodes, J.D., Webber, M.E., 2020. Understanding the impact of non-synchronous wind and solar generation on grid stability and identifying mitigation pathways. Appl. Energy 262, 114492.

Kaloi, G.S., Wang, J., Baloch, M.H., 2016. Active and reactive power control of the doubly fed induction generator based on wind energy conversion system. Energy Rep. 2, 194–200.

Mas'ud, A.A., et al., 2017. Wind power potentials in Cameroon and Nigeria: Lessons from South Africa. Energies 10 (4).

Modi, N., Saha, T.K., Anderson, T., 2013. Damping performance of the large scale Queensland transmission network with significant wind penetration. Appl. Energy 111, 225–233.

NERC, 2019. Nigerian electricity regulatory commission quarterly report: Second quarter.

Nigeria-Electricity-Regulatory-Commission, Electricity Distribution Companies (DisCos) in Nigeria, ed., 2019. http://www.nercng.org/index.php/contact/discos.

Noorollahi, Y., Itoi, R., Yousefi, H., Mohammadi, M., Farhadi, A., 2017. Modeling for diversifying electricity supply by maximizing renewable energy use in Ebino city southern Japan. Sustainable Cities Soc. 34, 371–384.

Ogunjuyigbe, A.S.O., Ayodele, T.R., Adetokun, B.B., 2017. Steady state analysis of wind-driven self-excited reluctance generator for isolated applications. Renew. Energy 114, 984–1004.

Ogunjuyigbe, A.S.O., Ayodele, T.R., Adetokun, B.B., Jimoh, A.A., 2016. Dynamic performance of wind-driven self-excited reluctance generator under varying wind speed and load. In: 2016 IEEE International Conference on Renewable Energy Research and Applications (ICRERA), pp. 506–511.

Raghavendran, C.R., Preetha Roselyn, J., Devaraj, D., 2020. Development and performance analysis of intelligent fault ride through control scheme in the dynamic behaviour of grid connected DFIG based wind systems. Energy Rep. 6, 2560–2576.
Rahimi, M., 2017. Coordinated control of rotor and grid sides converters in DFIG based wind turbines for providing optimal reactive power support and voltage regulation. Sustain. Energy Technol. Assess. 20, 47–57.
Shaaban, M., Petinrin, J.O., 2014. Renewable energy potentials in Nigeria: Meeting rural energy needs. Renew. Sustain. Energy Rev. 29, 72–84.
Waewsak, J., Kongruang, C., Gagnon, Y., 2017. Assessment of wind power plants with limited wind resources in developing countries: Application to Ko Yai in southern Thailand. Sustain. Energy Technol. Assess. 19, 79–93.
Wang, Y., Xu, L., Solangi, Y.A., 2020. Strategic renewable energy resources selection for Pakistan: Based on SWOT-Fuzzy AHP approach. Sustainable Cities Soc. 52, 101861.
Willenberg, D., Winkens, A., Linnartz, P., 2020. Impact of wind turbine generator technologies and frequency controls on the stable operation of medium voltage islanded microgrids. Electr. Power Syst. Res. 189, 106760.
Wiser, R., et al., 2016. Long-term implications of sustained wind power growth in the United States: Potential benefits and secondary impacts. Appl. Energy 179, 146–158.
Wu, Y.-K., Lee, T.-C., Hsieh, T.-Y., Lin, W.-M., 2016. Impact on critical clearing time after integrating large-scale wind power into Taiwan power system. Sustain. Energy Technol. Assess. 16, 128–136.
Wu, Z., et al., 2018. State-of-the-art review on frequency response of wind power plants in power systems. J. Mod. Power Syst. Clean Energy 6 (1), 1–16.
Xia, J., Dyśko, A., apos, J.O., 2015. Reilly, future stability challenges for the UK network with high wind penetration levels, (in En). IET Gener. Transm. Dist. 9 (11), 1160–1167.
Yan, R., Saha, T.K., Modi, N., Masood, N.-A., Mosadeghy, M., 2015. The combined effects of high penetration of wind and PV on power system frequency response. Appl. Energy 145, 320–330.
Yu, M., et al., 2016. Use of an inertia-less Virtual Synchronous Machine within future power networks with high penetrations of converters. In: 2016 Power Systems Computation Conference (PSCC), pp. 1–7.
Zhang, R., Ni, M., Shen, G.Q.P., Wong, J.K.W., 2019. An analysis on the effectiveness and determinants of the wind power Feed-in-Tariff policy at China's national-level and regional-grid-level. Sustain. Energy Technol. Assess. 34, 87–96.
Zou, Y., 2015. Induction generator in wind power systems. In: Recalde, R.I.G. (Ed.), Induction Motors - Applications, Control and Fault Diagnostics. IntechOpen.